Fluid Phase Equilibria 493 (2019) 67–77

Contents lists available at ScienceDirect

Fluid Phase Equilibria

journal homepage: www.elsevier.com/locate/fluid

Pore size distributions from extended Peng-Robinson equations of state for fluids confined in cylindrical and slit pores

Gabriel D. Barbosa [a], Leonardo Travalloni [a, *], Marcelo Castier [b], Frederico W. Tavares [a, c]

[a] Escola de Química, Universidade Federal do Rio de Janeiro, Rio de Janeiro, C.P. 68542, Brazil
[b] Chemical Engineering Program, Texas A&M University at Qatar, Doha, P.O. Box 23874, Qatar
[c] Programa de Engenharia Química – COPPE, Universidade Federal do Rio de Janeiro, Rio de Janeiro, C.P. 68542, Brazil

ARTICLE INFO

Article history:
Received 3 December 2018
Received in revised form
4 April 2019
Accepted 5 April 2019
Available online 11 April 2019

Keywords:
Pore size distribution
Peng-Robinson
Adsorption
Slit pore
Confined fluids

ABSTRACT

Adsorption is widely applied in several practical processes. Thus, the development of mathematical tools for modeling adsorption systems is remarkably relevant. In the past few years, we have extended commonly used equations of state to fluids confined in cylindrical pores and the obtained models were successful in describing the adsorption of pure fluids and mixtures. In this work, we follow our previous approach to extend the Peng-Robinson equation of state to fluids confined in slit pores, based on molecular simulations of structural properties of the confined fluid. Furthermore, we investigate the potential of this modeling to provide pore size distributions of cylindrical- and slit-pore solids from pure fluid adsorption data. Predictive calculations of mixture adsorption were carried out with the obtained pore size distributions and the modeling showed a good performance, comparable to predictions of density functional theory.

1. Introduction

Adsorption is widely applied to separation processes [1,2], chromatography [3,4], heterogeneous catalysis [5,6], optical coating [7,8], and in the development of corrosion-resistant materials [9,10]. Among the approaches for its mathematical modeling, molecular simulation (molecular dynamics and Monte Carlo methods) and quantum/classical density functional theory (DFT) are alternatives of remarkable accuracy. From a practical point of view, however, such approaches have substantial computational cost and, for this reason, are currently unsuitable for chemical process design. Thus, there is an interest in developing simpler models for adsorption phenomena and fluids confined in porous materials, such as analytical equations of state. Although equations of state provide less detailed information about confined fluids as compared to molecular simulation and DFT, they can give average compositional and volumetric properties and are orders of magnitude faster than these more rigorous alternatives.

Over the past few decades, several researchers have proposed equations of state for confined fluids, generally by extending bulk fluid models, such as cubic equations of state [11–17], the perturbed-chain statistical associating fluid theory [18,19], and the Gibbs-Helmholtz constrained equation [20]. Particularly [11], extended the Peng-Robinson equation of state to fluids confined in cylindrical pores, based on the generalized van der Waals theory and on molecular simulation data for structural properties of the confined fluid. Their model relates the thermodynamic behavior of the fluid with the pore size and two additional parameters for each fluid component, dependent on the interaction between fluid molecules and pore walls (molecule-wall interaction). Despite its simplicity, this model provided good correlations of pure fluid adsorption isotherms and good predictions of mixture adsorption behavior, without fitting binary interaction parameters. In recent work [12], a more consistent modeling of confined fluids was achieved by using explicit mixing rules. Additionally, this modeling approach was extended to spherical pores and it was shown that a proper confinement geometry assumption can favor the model performance. However, most of these calculations were based on the assumption of a single pore size for the adsorbent (generally an experimental mean size), neglecting any morphological heterogeneity of the solid. This is a limitation when dealing with a broad pore size distribution (PSD). For instance, shale rocks can have broad PSDs with multiple peaks in the micro-mesopore range, whose knowledge is required for a proper estimation of the fluid-in-place amount in shale gas and oil reservoirs [21].

* Corresponding author.
E-mail address: travalloni@eq.ufrj.br (L. Travalloni).

https://doi.org/10.1016/j.fluid.2019.04.007
0378-3812/

Much of the difficulty in modeling the adsorption of gases on porous media lies in the characterization of the adsorbent morphology (specific surface area, total pore volume, and PSD), which is important to optimize industrial adsorption processes. Traditionally, surface areas have been experimentally evaluated with the Brunauer-Emmett-Teller (BET) adsorption isotherm [22], while PSDs have been evaluated by the Barrett-Joyner-Halenda (BJH) method [23]. However, given the assumption of multiple adsorption layers underlying the BET isotherm and the use of the Kelvin equation by the BJH method, both methodologies may lead to significant errors for microporous structures. In a seminal paper [24], analyzed the structure of porous carbons using DFT and obtained more reliable PSD results when compared to the previously mentioned methods [25]. Since then, other works used this methodology to obtain PSDs of porous media [26–28]. Nonetheless, despite the advantages of DFT in morphological characterizations, artificial results for carbonaceous solids were reported [29,30], motivating the development of new DFT models [31,32].

In this work, the Peng-Robinson equation of state was extended to fluids confined in slit pores, following methodologies presented before for cylindrical pores [11,12], for the slit geometry is more representative of some porous solids, such as activated carbons and shale rocks [21]. Despite the empirical basis of the original Peng-Robinson equation of state, this model is widely used in the gas and oil industry, successfully describing the behavior of several bulk fluids (pure and mixed) with sufficient numerical simplicity for application in engineering tools, such as process simulators. The intended model should retain the simple mathematical nature of the Peng-Robinson equation of state and should reduce to this model in the bulk limit (i.e., for infinite pore size), so that the extended model could be easily included in available engineering tools to describe both bulk and confined fluids in a consistent way. In addition, although not done in this work, it should be possible to model fluid confinement in complex heterogeneous solids, whose void space can be approximated as a combination of slit, cylindrical, and spherical pores, by a simple summation of the adsorbed amounts in each pore geometry, calculated with the model version appropriate for each geometry.

To extend the Peng-Robinson equation of state to fluids confined in slit pores, Monte Carlo molecular simulations were carried out to provide structural data of the slit-confined fluid. Then, our confined fluid models were used in the calculation of PSDs of cylindrical- and slit-pore solids from pure fluid adsorption data. Predictive calculations of pure fluid and mixture adsorption were performed based on the obtained PSDs and results were compared to literature experimental/DFT data.

2. Formulation of the models

2.1. Equation of state for pure fluids in cylindrical pores

In previous work [11], the Peng-Robinson equation of state was extended to fluids confined in cylindrical pores based on molecular simulation data for structural properties of the confined fluid. The pressure-explicit expression for pure confined fluids is:

$$P = \frac{RT}{v - b_p} - \frac{a_p}{v^2 + 2b_p v - b_p^2} + \frac{RT\beta\gamma\vartheta^{b_4}(1 - F_{pp})}{(v - b_p)\left(1 + b_3\vartheta^{b_4}\right)^2} \tag{1}$$

with:

$$\beta = \frac{{b_1}^{1/b_2} b_3 b_4}{b_2} \tag{2}$$

$$\gamma = \Gamma\left[-\frac{1}{b_2}, b_1\left(\frac{RT}{N_{av}\varepsilon_p}\right)^{b_2}\right] \tag{3}$$

$$\vartheta = \frac{b_p}{v - b_p} \tag{4}$$

$$a_p = a\,h \tag{5}$$

$$b_p = \frac{N_{av}}{\rho_{max}} \tag{6}$$

where R is the ideal gas constant, T is the absolute temperature, v is the molar volume, N_{av} is the Avogadro number, ε_p is the molecule-wall interaction energy, a is the energy parameter of the bulk Peng-Robinson model, Γ is the upper incomplete gamma function:

$$\Gamma(s, y) = \int_y^\infty t^{s-1} exp(-t) dt \tag{7}$$

and ρ_{max}, h, F_{pp}, and b_1–b_4 are functions of the pore geometry and size. For cylindrical confinement, ρ_{max} is:

$$\rho_{max}\sigma^3 = c_1 - c_2 exp\left(c_3\left(0.5 - \frac{r_p}{\sigma}\right)\right) + c_4 exp\left(c_5\left(0.5 - \frac{r_p}{\sigma}\right)\right) \tag{8}$$

and the other geometry-dependent terms were fitted by Ref. [11] to their simulated data:

$$h = 1 - \frac{6}{7}\exp\left(-m_1\left(\frac{r_p}{\sigma} - 0.5\right)^{m_2}\right) \tag{9}$$

$$F_{pp} = F_{pr} + o_1(1 - F_{pr})\left(1 - \exp\left(-o_2\frac{\delta_p}{r_p}\right)\right) \tag{10}$$

$$b_k = C_{4k-3} + \frac{C_{4k-2}}{1 + C_{4k-1}(0.5 r_p/\delta_p)^{C_{4k}}}, \quad k = 1, 2, 3, 4 \tag{11}$$

where σ is the fluid molecule hardcore diameter, r_p is the pore radius, δ_p is the molecule-wall interaction range (beyond the

Table 1
Universal constants of Equations (8)–(11)) (for cylindrical confinement).

Equation (8)					Equation (9)		Equation (10)	
c_1	c_2	c_3	c_4	c_5	m_1	m_2	o_1	o_2
1.16	0.48	0.62	0.60	4.01	0.78	0.98	0.87	−2.22
Equation (11)								
C_1	C_2	C_3	C_4	C_5	C_6	C_7	C_8	
5899.89	11486.82	478.92	−2.34	7.71	0	0	0	
C_9	C_{10}	C_{11}	C_{12}	C_{13}	C_{14}	C_{15}	C_{16}	
0.00	73.67	1110.81	−2.38	1.99	0.00	0.00	0.00	

Table 2
Universal constants of Equations (13)–(16)) (for slit confinement).

Equation (13)							
c_1	c_2	c_3	c_4	c_5	c_6	c_7	c_8
1.15	20.03	2.78	0.45	−1.90	1.19	1.55	2.11
c_9	c_{10}	c_{11}	c_{12}	c_{13}			
6.15	0.38	0.86	1.65	9.03			
Equation (14)			Equation (15)				
m_1	m_2		o_1	o_2			
2.34	0.26		5.00	0.40			
Equation (16)							
C_1	C_2	C_3	C_4	C_5	C_6	C_7	C_8
191508.24	1529846.45	35.60	−1.12	10.86	0	0	0
C_9	C_{10}	C_{11}	C_{12}	C_{13}	C_{14}	C_{15}	C_{16}
0.00	99.32	1136.23	−2.11	1.06	717.83	383.24	0.30

hardcore repulsion distance), F_{pr} is given by:

$$F_{pr} = \frac{(r_p - \sigma/2)^2 - (r_p - \sigma/2 - \delta_p)^2}{(r_p - \sigma/2)^2} \tag{12}$$

and m_1, m_2, o_1, o_2, c_1–c_5, and C_1–C_{16} are universal parameters (Table 1). In this work, parameters C_1–C_{16} were refitted to the simulated data of [11] by setting $C_6 = 0$. In this way, term b_2 (Equation (11) for $k = 2$) was made constant for simplicity, with negligible loss of fit relative to the fit presented by Ref. [11].

Some of the terms presented here are detailed in the next sections. More detail on the model for cylindrical confinement is available elsewhere [11]. Moreover, some analytical details of the model derivation are presented in Appendix A, where we also provide the expression of the molar Helmholtz free energy, which can be used to obtain other thermodynamic properties, such as the chemical potential.

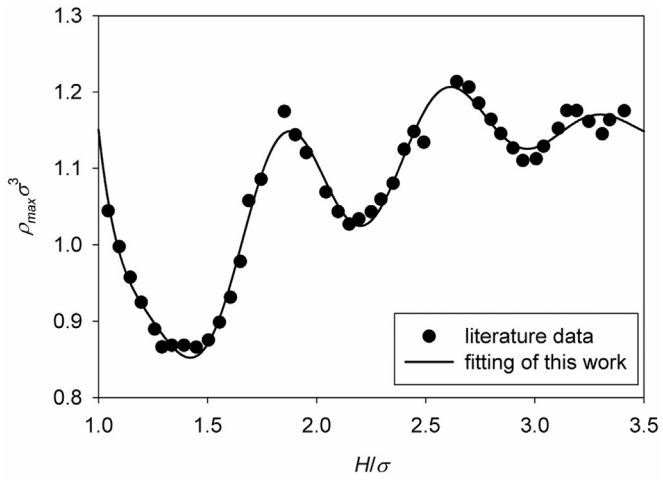

Fig. 1. Fitting of Equation (13) to simulation data [33] for the packing density of hard spheres as a function of the slit width.

2.2. Equation of state for pure fluids in slit pores

In this work, a Peng-Robinson-based model for pure fluids confined in slit pores was developed with the same methodology presented before for cylindrical pores [11]. Thus, the models obtained for both confinement geometries have similar formulations. For slit confinement, Equations (1)–(6) are maintained, while the geometry-dependent terms (Equations (8)–(12)) change to some extent.

The term ρ_{max} is the molecular packing density of the confined fluid, related to the repulsive part of the equation of state and its volume parameter [33]. reported simulation data for the close-packing fraction of hard spheres in a slit-like geometry as a function of the slit width. These data were converted to dimensionless packing densities and used to fit the empirical expression:

$$\rho_{max}\sigma^3 = c_1 + \sum_{k=1}^{3}\left(c_{4k-2}\exp\left(-c_{4k-1}\frac{H}{\sigma}\right)\cos\left(c_{4k}\frac{H}{\sigma} + c_{4k+1}\right)\right) \tag{13}$$

where H is the pore width and c_1–c_{13} are universal fitting

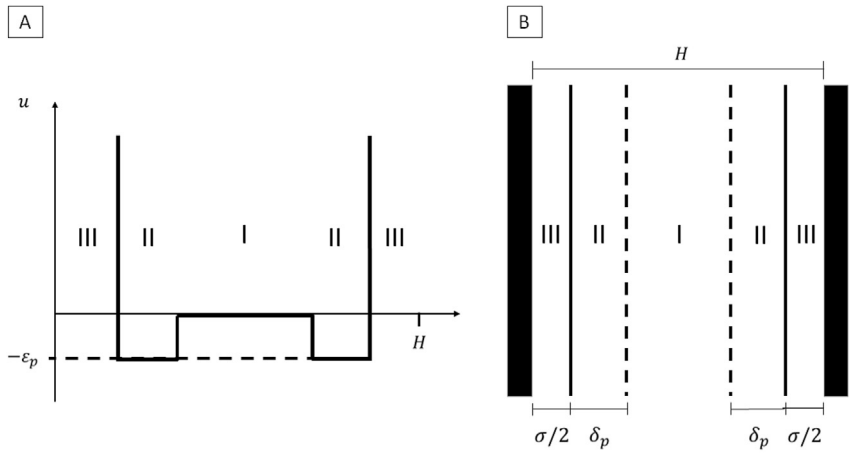

Fig. 2. (A) Molecule-wall interaction potential. (B) Corresponding regions inside a slit pore.

parameters (Table 2). Fig. 1 shows the fitting of Equation (13) to the simulation data of [33]. For consistency with the bulk Peng-Robinson equation of state, σ should be calculated from the volume parameter of this model and the bulk limit of Equation (13), c_1 [12]. The volume and energy parameters of the bulk Peng-Robinson model are calculated from the critical temperature, critical pressure, and acentric factor of the fluid.

The functions h, F_{pp}, and b_1–b_4 are related to the attractive part of the equation of state and its energy parameter. In order to obtain these functions for slit confinement, Grand Canonical Monte Carlo simulations were performed for a pure square-well fluid of spherical molecules in a slit-like simulation box with periodic boundary condition in the two coordinates parallel to the pore walls. The molecule-wall interaction was modeled by the square-well potential in Fig. 2A. This potential function (u) defines three regions (I, II, and III) inside a confining pore (Fig. 2B). Only in region II the fluid molecules are attracted to the pore walls. Structural properties of the confined fluid (coordination number and molecule distribution between pore regions I and II) were obtained for different pore widths ($H/\sigma = 5$–25), fluid densities ($\rho/\rho_{max} \approx 0$–$0.8$), and molecule-wall interaction energies ($\varepsilon_p/\varepsilon = 1$–$14.9$, where ε is the molecule-molecule interaction energy). The molecule-molecule interaction range beyond the hardcore repulsion distance (δ), the molecule-wall interaction range, and the temperature were kept constant ($\delta/\sigma = \delta_p/\sigma = 0.5$ and $kT/\varepsilon = 1.97$, where k is the Boltzmann constant). More information on the molecular simulation procedure is available elsewhere [11].

The simulation results for the structural properties of the slit-confined fluid revealed profiles qualitatively analogous to those observed for cylindrical confinement [11]. Thus, h, F_{pp}, and b_1–b_4 were fitted to the simulated data using expressions similar to Equations (9)–(11). This fitting is illustrated in the supplementary material.

The function h is a factor of reduction of the coordination number due to confinement:

$$h = 1 - \frac{5}{7}\exp\left(- m_1 \left(\frac{H}{2\sigma} - 0.5 \right)^{m_2} \right) \tag{14}$$

where m_1 and m_2 are universal fitting parameters (Table 2). Equation (14) was based on the maximum coordination number consistent with the bulk Peng-Robinson equation of state, which is about 14 [11], and on the assumption of a maximum coordination number of 4 in the extremely confined, two-dimensional fluid (for $H = \sigma$). In this limit, therefore, the coordination number is reduced to 2/7 of the bulk value.

The function F_{pp} is the fraction of the confined molecules that interact with the pore walls in the packing condition, i.e., the fraction of molecules in pore region II (Fig. 2B) when the fluid density is ρ_{max}. Similarly, the functions b_1–b_4 are related to the distribution of the fluid molecules inside the pore [11]. These functions were modeled by:

$$F_{pp} = F_{pr} + o_1 (1 - F_{pr}) \left(1 - \exp\left(- o_2 \frac{\delta_p}{H} \right) \right) \tag{15}$$

$$b_k = C_{4k-3} + \frac{C_{4k-2}}{1 + C_{4k-1} (0.5H/\delta_p)^{C_{4k}}}, \quad k = 1,\ 2,\ 3,\ 4 \tag{16}$$

where o_1, o_2, and C_1–C_{16} are universal fitting parameters (Table 2) and F_{pr} is the fraction of the confined molecules in pore region II for random distribution of the molecules throughout the pore, i.e., the ratio of the volume of region II to the combined volume of regions I and II in Fig. 2B:

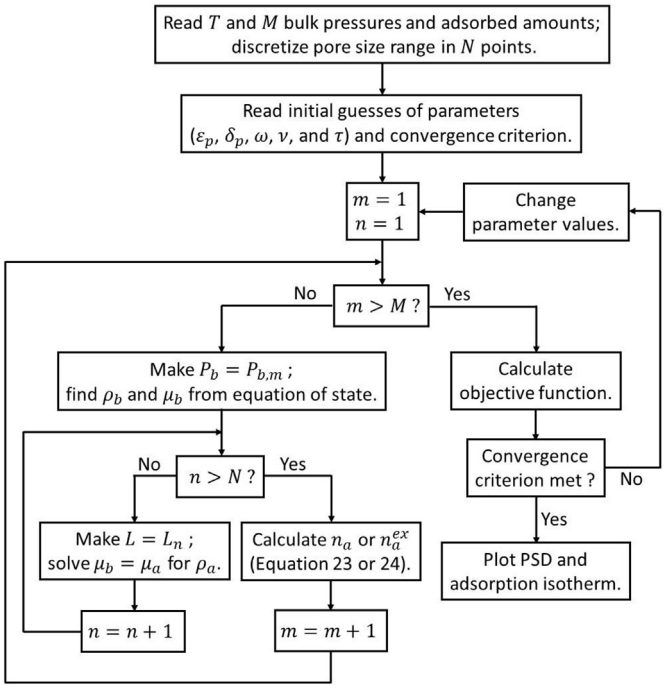

Fig. 3. Schematic representation of the parameter estimation procedure.

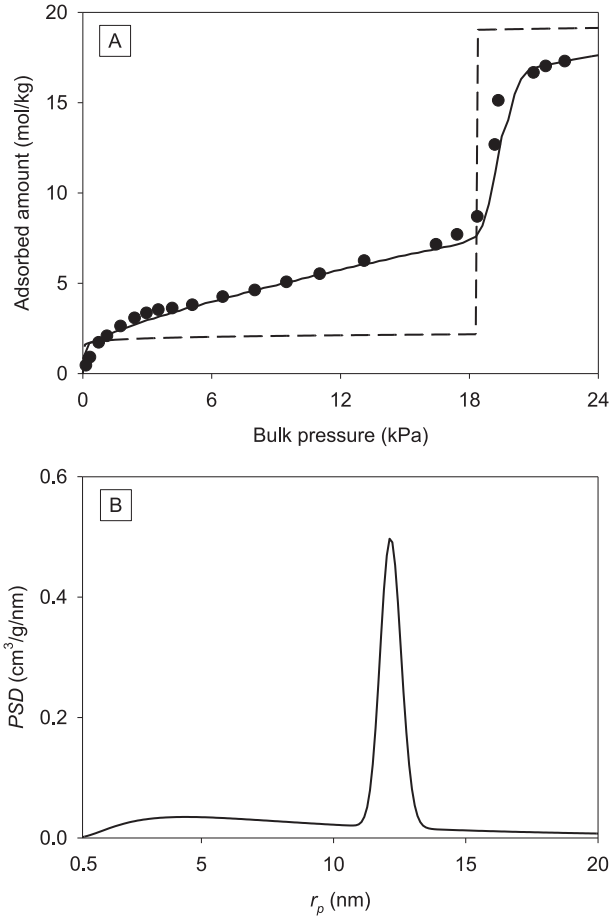

Fig. 4. (A) Pure methanol adsorption on molecular sieve MCM-48 at 313.15 K; symbols represent experimental data of [35]; the full line represents the PR-C model fit assuming a PSD, and the dashed line represents the model fit assuming a mean pore size (11.20 nm). (B) Adsorbent PSD from the PR-C model fit.

$$F_{pr} = \frac{2\delta_p}{H-\sigma} \tag{17}$$

2.3. Equations of state for fluid mixtures in cylindrical and slit pores

The extension of the pure confined fluid models to confined mixtures is performed here according to the consistent approach of [12]. In this way, mean, composition-dependent parameters are obtained for a mixture from one-fluid mixing rules and most of the equations presented in Sections 2.1 and 2.2 apply to the mixture as a whole. Exceptions are Equations (5), (6), (8) and (13). Particularly, Equations (8) and (13) (depending on the confinement geometry) still give the packing density of each pure component i ($\rho_{max,i}$), using the molecular diameter of this component (σ_i). Equations (5) and (6), which give the confinement-modified parameters of the Peng-Robinson equation of state for pure fluids, are replaced by:

$$a_p = h\sum_{i=1}^{NC}\sum_{j=1}^{NC}\left(x_i x_j \sqrt{a_i a_j}\right) \tag{18}$$

$$b_p = \sum_{i=1}^{NC}\left(x_i \frac{N_{av}}{\rho_{max,i}}\right) \tag{19}$$

where NC is the number of fluid components and x is the mole fraction (in Equation (18), the binary interaction parameters were omitted because they were not fitted in this work and mixture calculations were predictive). In the other equations of Sections 2.1 and 2.2, σ, ε_p, and δ_p become:

$$\sigma = \sum_{i=1}^{NC}(x_i\sigma_i) \tag{20}$$

$$\varepsilon_p = \sum_{i=1}^{NC}(x_i\varepsilon_{pi}) \tag{21}$$

$$\delta_p = \sum_{i=1}^{NC}(x_i\delta_{pi}) \tag{22}$$

With this formulation, both models reduce to the original Peng-Robinson equation of state when H/σ or r_p/σ tends to infinity (bulk fluid). Therefore, the models of this work can be applied to both bulk and confined phases, providing consistent adsorption calculations. Henceforth, the model for cylindrical confinement will be called PR-C (Equations (1)–(4)(8)–(12) and (8)–(22)) and the model for slit confinement will be called PR-S (Equations (1) and (1)–(4)3-22). The corresponding expressions for the chemical potential of a fluid component are more complex and are provided as FORTRAN calculation routines in the supplementary material.

Table 3
Molecule-wall interaction parameters (ε_p and δ_p) estimated from pure fluid adsorption data.

Reference	Adsorbent	Model	Adsorbate	σ(nm)	ε_p/k(K)	δ_p(nm)
[35]	MCM-48	PR-C	CH_3OH	0.429	5203.76	0.210
[37]	shale	PR-S	CO_2	0.371	1434.84	0.090
	08–154		CH_4	0.372	1228.30	0.058
[38]	shale	PR-S	CO_2	0.371	1514.66	0.120
	Barnett		CH_4	0.372	1315.68	0.113
[39]	carbon	PR-S	CO_2	0.371	1272.98	0.254
	Maxsorb		CH_4	0.372	1211.74	0.252
[40]	carbon	PR-S	CO_2	0.371	1695.10	0.143
	Norit		CH_4	0.372	1574.92	0.140
	R1		N_2	0.358	1493.77	0.091
[41]	carbon	PR-S	CO_2	0.371	1706.52	0.162
	Filtrasorb		CH_4	0.372	1617.84	0.147
	400		N_2	0.358	1591.52	0.097

Table 4
PSD parameters (ω, ν, and τ) estimated from pure fluid adsorption data and pore volumes obtained from Equation (26).

Reference	Adsorbent	V_p(cm^3/g)	$\omega \times 10^6$	Peak	ν	τ
[35]	MCM-48	0.874	0.608	1	−18.51	0.858
				2	−18.22	0.032
[37]	shale	0.013	0.004	1	−20.49	0.123
	08–154			2	−19.38	0.307
				3	−17.83	0.110
[38]	shale	0.027	0.009	1	−19.30	0.053
	Barnett			2	−19.03	0.132
				3	−18.96	0.108
				4	−18.92	0.040
[39]	carbon	1.269	0.423	1	−20.14	0.582
	Maxsorb			2	−19.79	0.469
				3	−19.04	0.464
[40]	carbon	0.407	0.407	1	−20.47	0.341
	Norit					
	R1					
[41]	carbon	0.316	0.316	1	−20.35	0.294
	Filtrasorb					
	400					

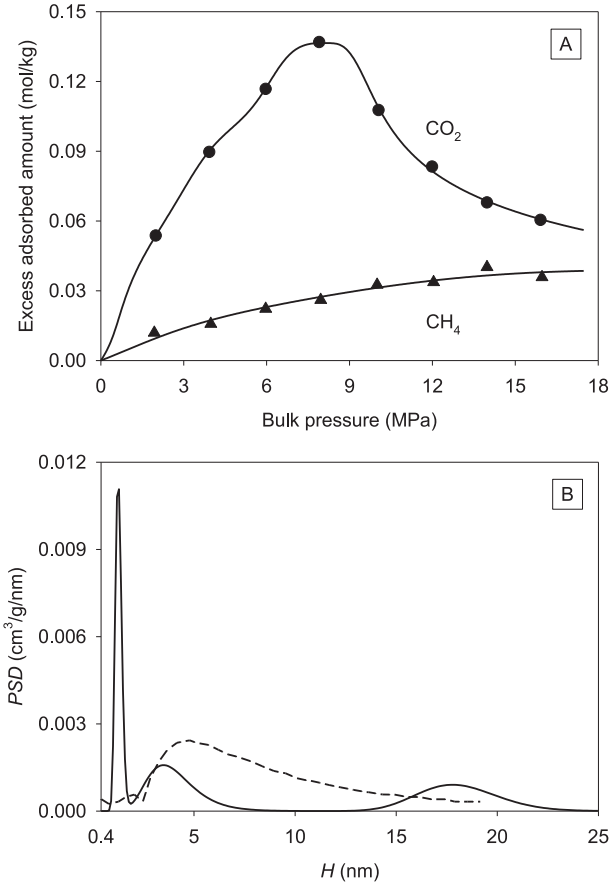

Fig. 5. (A) Pure carbon dioxide and methane adsorption on shale rock 08–154 at 318.15 K; symbols represent experimental data of [37] and lines represent the PR-S model fits. (B) Adsorbent PSDs; the full line represents the PR-S model fit and the dashed line represents the DFT result of [21].

3. Calculation of PSD with the equations of state

The PSDs of cylindrical- and slit-like porous media were calculated from pure fluid adsorption isotherms, based on the PR-C and PR-S models (Section 2). Given a PSD, the total or the excess adsorbed amount of a fluid is obtained from the weighted contributions of the individual pore sizes:

$$n_a = \int_{L_{min}}^{L_{max}} PSD(L)\rho_a(L)dL \tag{23}$$

$$n_a^{ex} = \int_{L_{min}}^{L_{max}} PSD(L)(\rho_a(L) - \rho_b)dL \tag{24}$$

where L is the pore size (r_p or H, depending on the confinement geometry), L_{min} and L_{max} are the lower and upper limits of the PSD, respectively, and ρ_a and ρ_b are the molar densities of the adsorbed and bulk phases, respectively. For each point in an adsorption isotherm, the temperature and the bulk pressure are specified and the Peng-Robinson equation of state gives ρ_b, while ρ_a is calculated from the adsorption equilibrium condition (the equality of chemical potentials between both phases). The equilibrium condition can be solved for the models of this work as long as one knows the pore size and the molecule-wall interaction parameters ($\varepsilon_{p,i}$ and $\delta_{p,i}$). This adsorption calculation was detailed elsewhere [16]. With ρ_a for each pore size of the PSD, the adsorbed amount can be calculated from Equations (23) and (24)).

The PSD was modeled by a combination of log-normal distributions [21]:

$$PSD(L) = \frac{\omega}{L\sqrt{2\pi}} \sum_{k=1}^{NP} \left(\frac{1}{\tau_k} \exp\left(-\frac{(\ln(L) - \nu_k)^2}{2\tau_k^2} \right) \right) \tag{25}$$

where NP is the number of peaks in the PSD and ω, τ, and ν are fitting parameters (ω is related to the total pore volume and τ and ν are parameters characteristic of the log-normal distribution function). As long as one knows these parameters, the total pore volume and the mean pore size can be obtained from the PSD by the

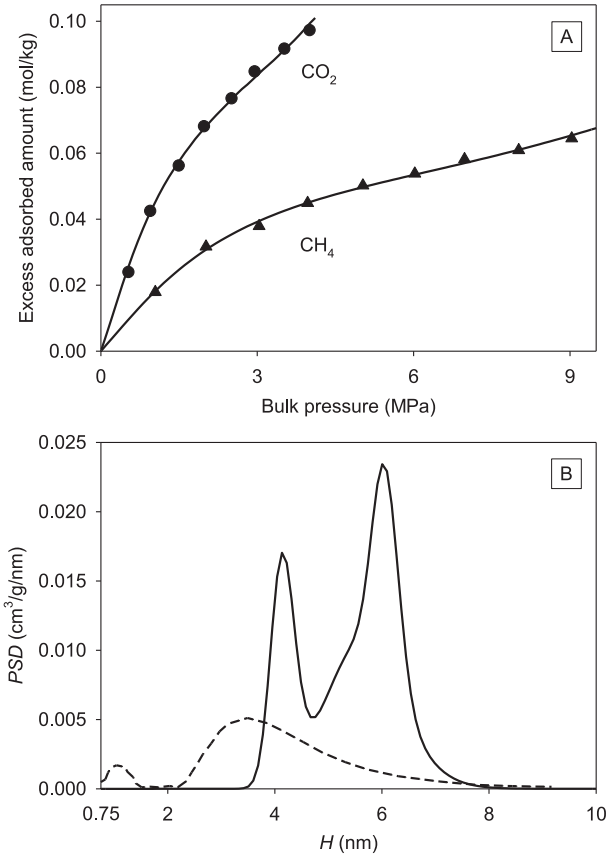

Fig. 6. (A) Pure carbon dioxide and methane adsorption on shale rock Barnett at 313.15 K; symbols represent experimental data of [38] and lines represent the PR-S model fits. (B) Adsorbent PSDs; the full line represents the PR-S model fit and the dashed line represents the DFT result of [21].

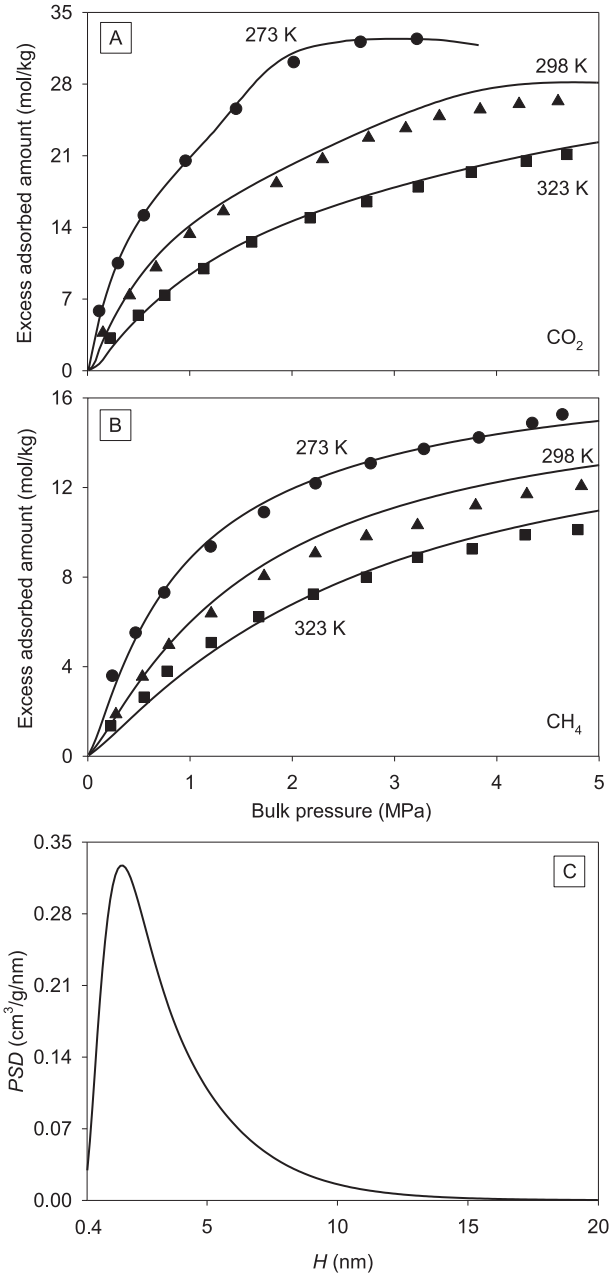

Fig. 7. (A) Pure carbon dioxide adsorption on activated carbon Maxsorb at 273 K; symbols represent experimental data of [39] and lines represent the PR-S model fits (for the lowest temperature) or model predictions (for the other temperatures). (B) Same as (A) for methane. (C) Adsorbent PSD from the PR-S model fit.

following equations, respectively:

$$V_p = \int_{L_{min}}^{L_{max}} PSD(L)dL \tag{26}$$

$$\overline{L} = \int_{L_{min}}^{L_{max}} \frac{PSD(L)\,L}{V_p} dL \tag{27}$$

The PSD parameters and the molecule-wall interaction parameters were simultaneously fitted to experimental adsorption data using the particle swarm optimization method [34] with the least squares objective function. The number of peaks in the PSD was varied to provide a satisfactory model fit to each evaluated adsorption isotherm. The integrations in Equations (23), (24), (26) and (27) were performed using the trapezoidal method with 200 equally-spaced points within the integration range. The upper limit of this range was within 50–80 σ, where σ is the molecule diameter of the fluid whose adsorption data were used for parameter estimation. The lower limit of the integration range was 0.6 σ for cylindrical confinement and 1.1 σ for slit confinement, near the extreme confinement limits (which are 0.5 σ and 1 σ, respectively). Fig. 3 shows a schematic representation of the parameter estimation procedure.

Based on the obtained PSDs, predictive calculations of mixture adsorption were performed. In these calculations, the bulk conditions (temperature, pressure, and composition) are specified and the adsorbed phase properties (density and composition) are calculated from the adsorption equilibrium equations for all components [16]. Then, the adsorbed amount of each component is obtained from:

$$n_{a,i} = \int_{L_{min}}^{L_{max}} PSD(L)x_{i,a}(L)\rho_a(L)dL \tag{28}$$

4. Results of PSD and adsorption calculations

Initially, the PR-C model was used to evaluate the effect of the PSD estimation on the correlation of a pure fluid adsorption isotherm. This evaluation was based on experimental data of methanol adsorption on MCM-48 molecular sieve [35], whose pores can be reasonably approximated as cylindrical [36]. Fig. 4 shows these experimental data, the model fit, and the corresponding PSD. The estimated model parameters are presented in Table 3 and the estimated PSD parameters (including the pore volume) are presented in Table 4. By fitting a bimodal PSD, the model provided a good correlation of the adsorption isotherm, which is of type-IV in the IUPAC classification [42]. Also according

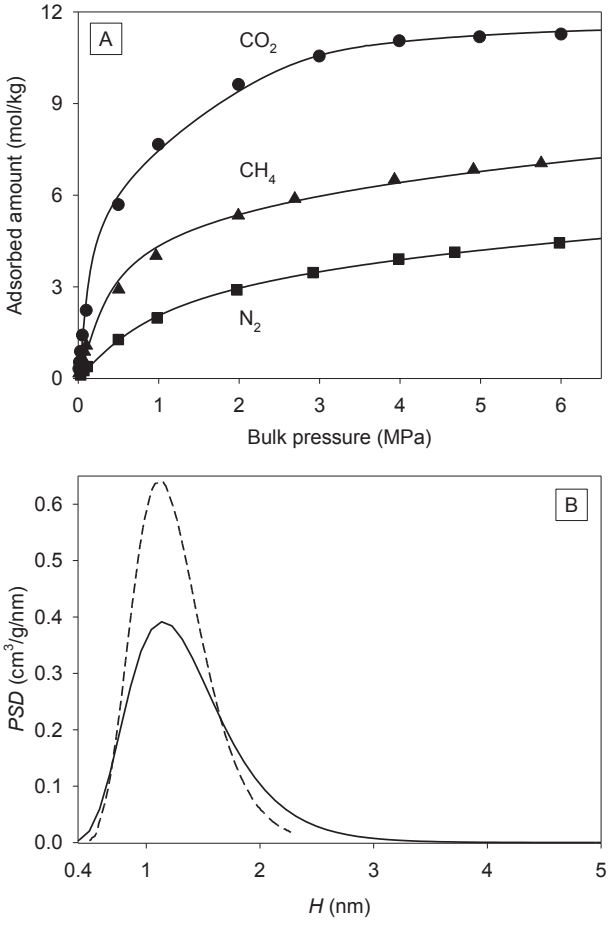

Fig. 8. (A) Pure carbon dioxide, methane, and nitrogen adsorption on activated carbon Norit R1 at 298 K; symbols represent experimental data of [40] and lines represent the PR-S model fits. (B) Adsorbent PSDs; the full line represents the PR-S model fit and the dashed line represents the DFT result of [45].

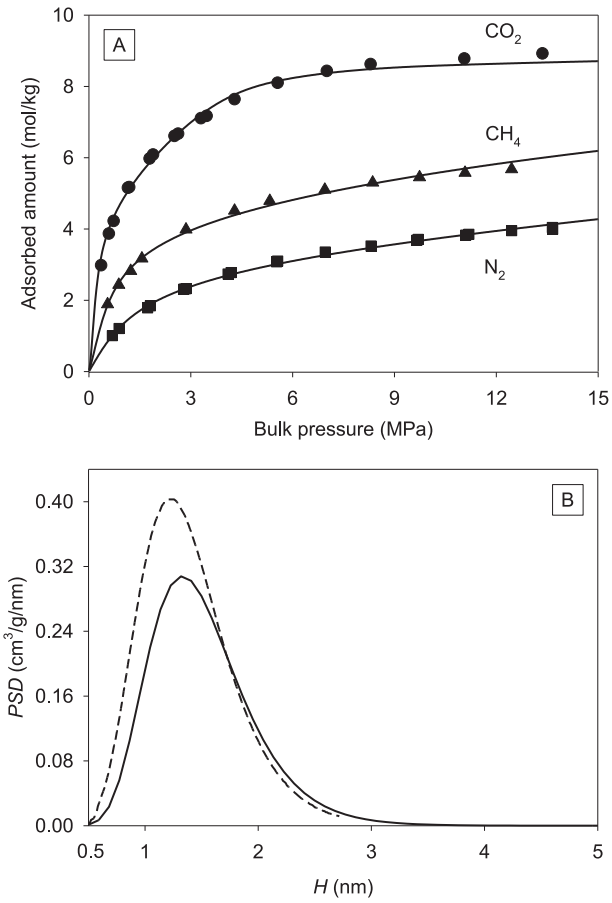

Fig. 9. (A) Pure carbon dioxide, methane, and nitrogen adsorption on activated carbon Filtrasorb 400 at 318.2 K; symbols represent experimental data of [41] and lines represent the PR-S model fits. (B) Adsorbent PSDs; the full line represents the PR-S model fit and the dashed line represents the DFT result of [45].

to the IUPAC [43], the estimated PSD is mostly in the mesopore range (widths between 2 and 50 nm characterize mesopores, while micropore widths are below that range).

For comparison with the PSD estimation procedure, the adsorption data in Fig. 4 were also correlated by the simpler approach of our previous work [11,12,16], based on a mean pore radius. This mean pore size was calculated from the obtained PSD (11.20 nm) and used together with the obtained pore volume to re-estimate the molecule-wall interaction parameters. The resulting fit is also shown in Fig. 4. With a single pore size instead of a PSD, the PR-C model failed to correlate the data due to the emergence of an adsorbed phase transition, instead of the continuous experimental profile. However, this phase transition was coherently located at the edge of the capillary condensation region. For describing a continuous profile in this region, a PSD is necessary because a pure fluid in a single pore size at a specified temperature undergoes phase transition at a unique bulk pressure, according to the Gibbs phase rule. Additionally, the model fitting was repeated using the adsorbent properties reported by Ref. [35]; obtained with the BJH method (r_p = 1.6 nm, V_p = 1.08 cm^3/g). The resulting fit (not shown) was similar to that for the mean pore size estimated here. Therefore, even the estimation of simple PSDs can play a significant role in the correlation of relatively complex adsorption isotherms.

Moreover, Fig. 4 shows that our model not only can predict the properties of each phase type (bulk and confined), but can also predict the phase equilibrium condition inside the pores and its deviation from the bulk condition. In the dashed line, the sudden increase in the adsorbed amount at about 19 kPa marks the transition from a vapor-like to a liquid-like confined phase, while the bulk vapor-liquid transition occurs at about 35 kPa for the specified temperature (313.15 K). Similarly, our modeling approach can predict deviations in other fluid properties, such as PVT behavior and phase equilibria.

Henceforth, the PSDs of slit-pore solids were calculated from pure fluid adsorption data of the literature using the PR-S model. As these data refer to more than one adsorbate, the adsorption isotherm of carbon dioxide was used in all cases to fit the PSD parameters, together with the molecule-wall interaction parameters of that adsorbate. Then, the molecule-wall interaction parameters of the other adsorbates were estimated using the already obtained PSD (excluding pore sizes below the diameters of these molecules, if necessary) [44]. performed molecular simulations of shale gas adsorption and observed that the accessible pore volume is related to the probing molecule. In this way, the PSD estimation can be affected by the choice of the adsorbate used for this purpose. However, this effect was neglected here because the addressed adsorbates have similar molecular diameters and the porous structure is assumed rigid.

Figs. 5 and 6 show excess adsorbed amounts of pure carbon dioxide and methane in different shale rocks [37,38] and the correlation of these experimental data with the PR-S model, including the respective PSDs. Shale rocks have inorganic and organic constituents and both contribute to gas sorption. However, for shale samples with low organic contents, the contribution from gas dissolution in the organic matter can be neglected [21]. Hence, the mentioned data were correlated considering a prevalent contribution of gas adsorption on the mineral part of the samples. The estimated parameters are presented in Tables 3 and 4. Excellent fittings were obtained (especially for the nonmonotonic adsorption isotherm of carbon dioxide in Fig. 5A), with essentially bi- or tri-modal PSDs in the micro-mesopore range. The obtained PSD in Fig. 6 resembles the DFT result of [21]; although their peaks are lower than ours (i.e., their pore volume is smaller) and their PSD is shifted by about 3 nm to lower pore sizes.

Fig. 7 shows excess adsorbed amounts of pure carbon dioxide

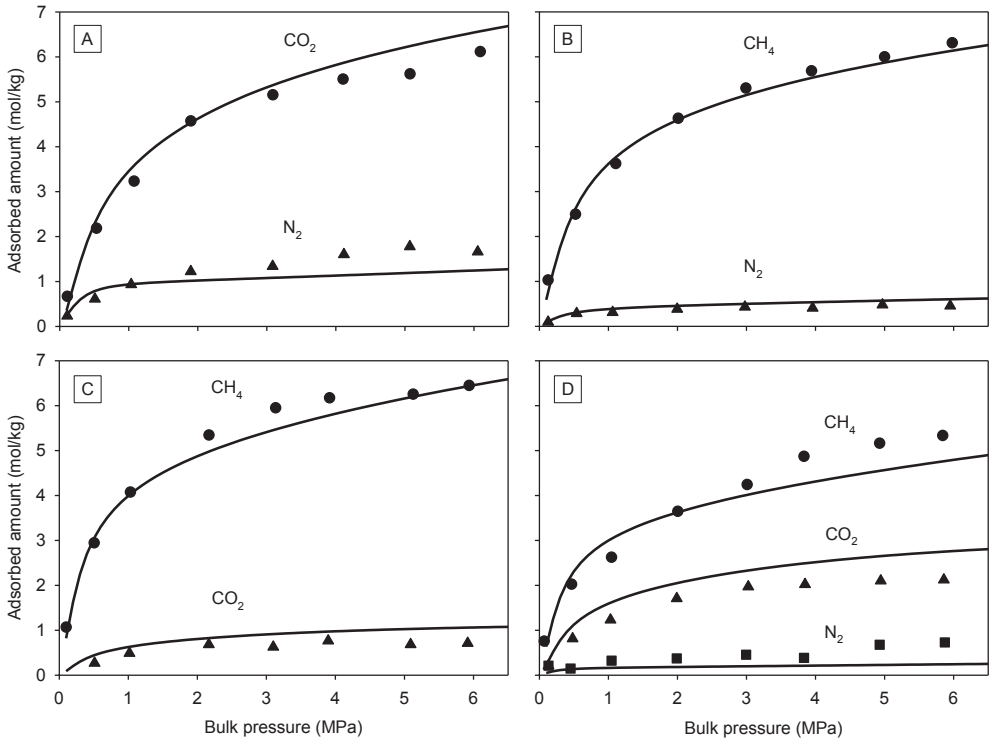

Fig. 10. Mixture adsorption on activated carbon Norit R1 at 298 K; symbols represent experimental data of [40] and lines represent the PR-S model predictions. (A) Binary mixture of CO_2 and N_2 with bulk composition x_{CO_2} = 0.20. (B) Binary mixture of CH_4 and N_2 with bulk composition x_{CH_4} = 0.72. (C) Binary mixture of CH_4 and CO_2 with bulk composition x_{CH_4} = 0.95. (D) Ternary mixture of CH_4, CO_2, and N_2 with bulk composition x_{CH_4} = 0.72 and x_{CO_2} = 0.12.

and methane in activated carbon [39] and the PR-S model fit to the data at 273 K. This figure also presents model predictions for higher temperatures (up to 323 K) based on the parameters estimated at 273 K (Tables 3 and 4). A good performance was obtained in both fit and predictions of the pure fluid adsorption isotherms. In this case, the evaluated PSD is essentially unimodal, centered in the micropore range.

Figs. 8 and 9 show the adsorption of pure carbon dioxide, methane, and nitrogen on different activated carbons [40,41] and the correlation of these experimental data with the PR-S model. Again, very good fits were obtained in both cases, together with unimodal PSDs centered in the micropore range. These PSDs are quite similar to the DFT results of [45] with respect to peak position, shape, and width, though our peaks are lower. Based on the obtained PSDs and the molecule-wall interaction parameters estimated for the pure fluids (Tables 3 and 4), predictions of binary and ternary mixture adsorption were carried out with the PR-S model (Figs. 10 and 11) and compared with the respective experimental data. Good predictions were obtained in most cases, with larger deviations for the ternary mixture (Fig. 10D) and the mixture of nitrogen and carbon dioxide in Fig. 11A. The model proposed here presented a prediction performance comparable to that of the DFT model used by Ref. [45].

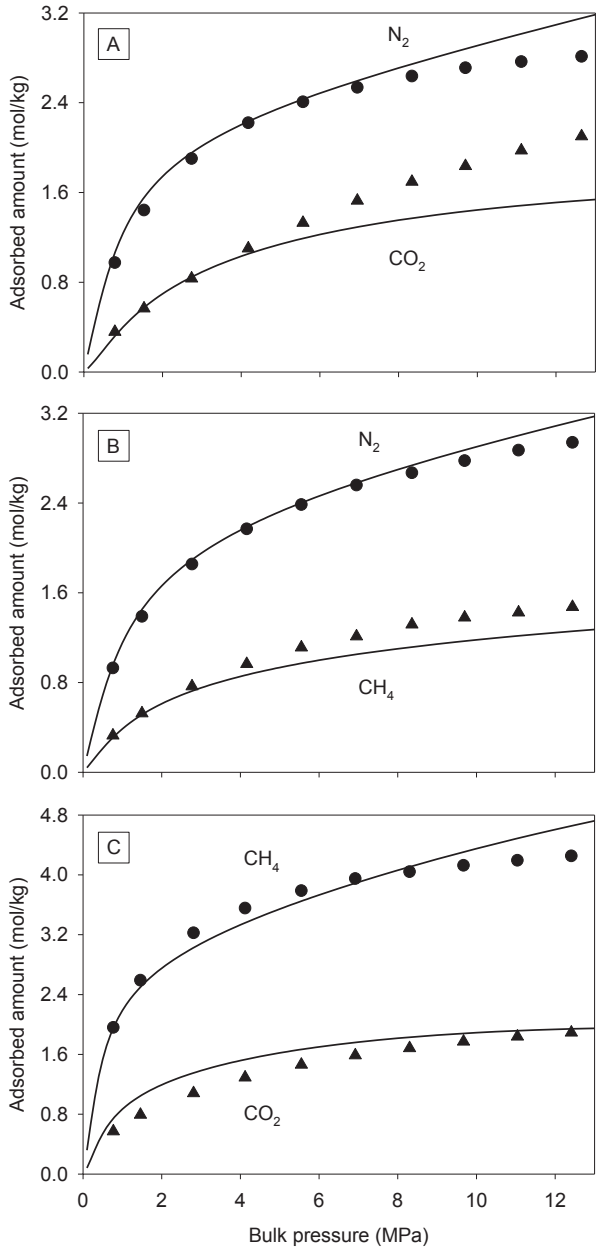

Fig. 11. Mixture adsorption on activated carbon Filtrasorb 400 at 318.2 K; symbols represent experimental data of [41] and lines represent the PR-S model predictions. (A) Binary mixture of N_2 and CO_2 with bulk composition $x_{N_2} = 0.94$. (B) Binary mixture of N_2 and CH_4 with bulk composition $x_{N_2} = 0.88$. (C) Binary mixture of CH_4 and CO_2 with bulk composition $x_{CH_4} = 0.87$.

5. Conclusions

In this work, the Peng-Robinson equation of state was extended to the confinement in slit-like porous media based on molecular simulation data of structural properties of the confined fluid. The extended model was intended to keep consistency with the bulk limit, i.e., the original Peng-Robinson equation of state is recovered when the pore size grows up indefinitely. The obtained model was used to evaluate PSDs of different solids from pure fluid adsorption data and some profiles showed qualitative similarities to DFT results. With the PSD estimation, the modeling showed a good performance in the correlation of pure fluid adsorption isotherms, including relatively complex profiles. For instance, a type IV isotherm was well correlated with a bimodal PSD, while the correlation failed with a single pore size. Therefore, the correlation ability of the modeling can be favored even with simple PSDs, compared to using pore size and volume data provided by the BET and BJH methods, which rely on different, simpler assumptions. Furthermore, the model showed a generally good performance in the prediction of mixture adsorption at high pressures, with results comparable to available DFT predictions. The presented approach is relevant to the modeling of gas and oil confined in shale reservoirs, which can have complex PSDs in the micro-mesopore range.

Acknowledgments

We acknowledge the financial support of CNPq, CAPES, ANP, and Petrobras (Brazil). The participation of M. Castier in this work was made possible by grant NPRP 8-1648-2-688 from the Qatar National Research Fund (a member of Qatar Foundation). The statemSents made herein are solely the responsibility of the authors.

Appendix A. Theoretical basis of the models

Following the generalized van der Waals theory [46], the canonical partition function of a mixture is:

$$Q(T,V,N_1,\ldots N_{NC}) = \prod_{i=1}^{NC}\left(\frac{q_i^{N_i}}{\lambda_i^{3N_i}N_i!}\right)V_f^N \exp\left(\int_\infty^T \frac{E_{conf}}{kT^2}\,dT\right) \tag{A.1}$$

where V is the total volume, N is the number of molecules, q is the internal partition function of one molecule, λ is the de Broglie wavelength, V_f is the free volume, E_{conf} is the configurational energy, and subscript i represents the ith component. To keep consistency with cubic equation of states, the free volume is:

$$V_f = V - \sum_{i=1}^{NC}\left(\frac{N_i}{\rho_{max,i}}\right) \tag{A.2}$$

The configurational energy includes the contribution of intermolecular interactions, under the assumption of pairwise additivity

(first term on the right hand side of Equation (A.3)), and the contribution of the interactions between the molecules of the mixture and the pore wall (second term on the right hand side of Equation (A.3)). Thus, the configurational energy is:

$$E_{conf} = h\sum_{i=1}^{NC}\sum_{j=1}^{NC}\left(-\frac{N_j}{2}N_{c,ij}\sqrt{\varepsilon_i\varepsilon_j}\right) - NF_p\varepsilon_p \quad (A.3)$$

where N_c is the coordination number for the bulk fluid, consistent with the Peng-Robinson equation of state [47], and F_p is the fraction of the mixture molecules within the attractive range of the confining wall. The expressions of N_c and F_p are provided in the supplementary material.

Starting from these equations, the derivation of the model involves making assumptions and approximations that allow the development of analytical expressions for $\rho_{max,i}$, h, and F_p, which depend on a pre-defined pore geometry (e.g., cylindrical, spherical, or slit-like). Ultimately, this allows the development of an analytical expression for the canonical partition function. Details of these assumptions and approximations are available in the literature [11,12,16].

Given the partition function (Equation (A.1)), all thermodynamic properties are promptly obtained. Particularly relevant to this work is the Helmholtz free energy, which is given by:

$$F = -kT\,lnQ \quad (A.4)$$

Explicitly, according to our approach, the molar Helmholtz free energy is:

$$f = RT\left(\sum_{i=1}^{NC}x_i\ln\left(\frac{N_{av}x_i\lambda_i^3}{q_i}\right) - \ln(v-b_p) - 1\right) - \frac{a_p}{2\sqrt{2}b_p}\ln\left(\frac{v+\left(1+\sqrt{2}\right)b_p}{v+\left(1-\sqrt{2}\right)b_p}\right) - N_{av}\varepsilon_p F_{pp} - \frac{RT\gamma b_1^{1/b_2}\left(1-F_{pp}\right)}{b_2\left(1+b_3\vartheta^{b_4}\right)} \quad (A.5)$$

which is the key property for obtaining the other thermodynamic properties, such as the chemical potential:

$$\mu_i = \left(\frac{\partial F}{\partial N_i}\right)_{T,V,N_{j\neq i}} \quad (A.6)$$

List of symbols

a	energy parameter of the bulk Peng-Robinson equation of state
a_p	Peng-Robinson energy parameter modified by confinement
b_1–b_4	functions of pore geometry and/or size
b_p	Peng-Robinson volume parameter modified by confinement
E_{conf}	configurational energy
f	molar Helmholtz free energy
F	total Helmholtz free energy
F_p	fraction of the confined molecules interacting with the pore walls
F_{pp}	fraction of the confined molecules interacting with the pore walls in the packing condition
F_{pr}	fraction of the confined molecules interacting with the pore walls for random distribution
h	function of pore geometry and size
H	slit pore width
k	Boltzmann constant
L	generic pore size
$\overline{L}$	mean pore size
L_{max}	upper limit of the pore size distribution
L_{min}	lower limit of the pore size distribution
n_a	total adsorbed amount
n_a^{ex}	excess adsorbed amount
N	number of molecules
N_{av}	Avogadro number
N_c	coordination number
NC	number of fluid components
NP	number of peaks in the pore size distribution
P	pressure
PSD	pore size distribution
q	internal partition function
Q	canonical partition function
R	ideal gas constant
r_p	cylindrical pore radius
T	temperature
u	molecule-wall interaction potential
v	molar volume
V	total volume
V_f	free volume
V_p	total pore volume
x	mole fraction

Greek letters

β	auxiliary term in the model equations
γ	auxiliary term in the model equations
Γ	upper incomplete gamma function
δ	square-well width of the molecule-molecule interaction potential
δ_p	square-well width of the molecule-wall interaction potential
ε	square-well depth of the molecule-molecule interaction potential
ε_p	square-well depth of the molecule-wall interaction potential
ϑ	auxiliary term in the model equations
λ	de Broglie wavelength
μ	chemical potential
ν	fitting parameter of the pore size distribution
ρ	molar density
ρ_{max}	molecular packing density
σ	molecular diameter
τ	fitting parameter of the pore size distribution
ω	fitting parameter of the pore size distribution

Subscripts

a	adsorbed phase
b	bulk phase
i, j	fluid component

Appendix B. Supplementary data

Supplementary data to this article can be found online at https://doi.org/10.1016/j.fluid.2019.04.007.

References

[1] X.-J. Hou, P. He, H. Li, X. Wang, Understanding the adsorption mechanism of C_2H_2, CO_2, and CH_4 in isostructural metal-organic frameworks with coordinatively unsaturated metal sites, J. Phys. Chem. C 117 (2013) 2824–2834.

[2] C. Sun, B. Xiong, Y. Pan, H. Cui, Adsorption removal of tannic acid from aqueous solution by polyaniline: analysis of operating parameters and mechanism, J. Colloid Interface Sci. 487 (2017) 175–181.
[3] J.E. Basconi, G. Carta, M.R. Shirts, Effects of polymer graft properties on protein adsorption and transport in ion exchange chromatography: a multiscale modeling study, Langmuir 31 (2015) 4176–4187.
[4] Y. Li, E. Pearce, J.W. Lyons, D. Murray, T. Chatterjee, D.M. Meunier, Fundamental study of the separation of homopolymers from block copolymers by liquid chromatography with preloaded adsorption promoting barriers, J. Chromatogr. A 1475 (2016) 41–54.
[5] J.C. Gee, S. Fisher, Direct esterification of olefins: the challenge of mechanism determination in heterogeneous catalysis, J. Catal. 331 (2015) 13–24.
[6] A.J. Medford, A. Vojvodic, J.S. Hummelshøj, J. Voss, F. Abild-Pedersen, F. Studt, T. Bligaard, A. Nilsson, J.K. Nørskov, From the Sabatier principle to a predictive theory of transition-metal heterogeneous catalysis, J. Catal. 328 (2015) 36–42.
[7] N. Hidalgo, M.E. Calvo, S. Colodrero, H. Miguez, Porous one-dimensional photonic crystal coatings for gas detection, IEEE Sens. J. 10 (2010) 1206–1212.
[8] X. Ling, G. Wang, Y. Zhao, X. Liu, J. Shao, Laser-induced damage of the optical coatings due to organic contamination in vacuum, Appl. Surf. Sci. 270 (2013) 346–351.
[9] R. Puthalath, A.O. Surendranathan, C.S.N. Murthy, Protective performance of furfuryl alcohol on 13Cr L80 steel against corrosion in hydrochloric acid solution, Ind. Eng. Chem. Res. 53 (2014) 23–30.
[10] R. Rosliza, W.B. Wan Nik, S. Izman, Y. Prawoto, Anti-corrosive properties of natural honey on Al-Mg-Si alloy in seawater, Curr. Appl. Phys. 10 (2010) 923–929.
[11] G.D. Barbosa, L. Travalloni, M. Castier, F.W. Tavares, Extending an equation of state to confined fluids with basis on molecular simulations, Chem. Eng. Sci. 153 (2016) 212–220.
[12] G.D. Barbosa, M.L. D'Lima, S.M.H. Daghash, M. Castier, F.W. Tavares, L. Travalloni, Cubic equations of state extended to confined fluids: new mixing rules and extension to spherical pores, Chem. Eng. Sci. 184 (2018) 52–61.
[13] X. Dong, H. Liu, J. Hou, K. Wu, Z. Chen, Phase equilibria of confined fluids in nanopores of tight and shale rocks considering the effect of capillary pressure and adsorption film, Ind. Eng. Chem. Res. 55 (2016) 798–811.
[14] A. Giaya, R.W. Thompson, Water confined in cylindrical micropores, J. Chem. Phys. 117 (2002) 3464–3475.
[15] M. Schoen, D.J. Diestler, Analytical treatment of a simple fluid adsorbed in a slit-pore, J. Chem. Phys. 109 (1998) 5596–5606.
[16] L. Travalloni, M. Castier, F.W. Tavares, S.I. Sandler, Thermodynamic modeling of confined fluids using an extension of the generalized van der Waals theory, Chem. Eng. Sci. 65 (2010) 3088–3099.
[17] G.J. Zarragoicoechea, V.A. Kuz, Van der Waals equation of state for a fluid in a nanopore, Phys. Rev. 65 (2002), 021110-1–4.
[18] L.F.M. Franco, I.G. Economou, M. Castier, Statistical mechanical model for adsorption coupled with SAFT-VR Mie equation of state, Langmuir 33 (2017) 11291–11298.
[19] S.P. Tan, M. Piri, Equation-of-state modeling of confined-fluid phase equilibria in nanopores, Fluid Phase Equilib. 393 (2015) 48–63.
[20] E. Thomas, A. Lucia, Multi-scale equation of state computations for confined fluids, Comput. Chem. Eng. 107 (2017) 16–25.
[21] Z. Jin, A. Firoozabadi, Thermodynamic modeling of phase behavior in shale media, SPE J. 21 (2016) 190–207.
[22] S. Brunauer, P.H. Emmett, E. Teller, Adsorption of gases in multimolecular layers, J. Am. Chem. Soc. 60 (1938) 309–319.
[23] E.P. Barrett, L.G. Joyner, P.P. Halenda, The determination of pore volume and area distributions in porous substances: I. Computations from nitrogen isotherms, J. Am. Chem. Soc. 73 (1951) 373–380.
[24] N.A. Seaton, J. Walton, N. Quirke, A new analysis method for the determination of the pore size distribution of porous carbons from nitrogen adsorption measurements, Carbon 27 (1989) 853–861.
[25] J. Landers, G.Y. Gor, A.V. Neimark, Density functional theory methods for characterization of porous materials, Colloids Surf., A 437 (2013) 3–32.
[26] A. Carati, G. Ferraris, M. Guidotti, G. Moretti, R. Psaro, C. Rizzo, Preparation and characterization of mesoporous silica-alumina and silica-titania with a narrow pore size distribution, Catal. Today 77 (2003) 315–323.
[27] A.V. Neimark, P.I. Ravikovitch, M. Grün, F. Schüth, K.K. Unger, Pore size analysis of MCM-41 type adsorbents by means of nitrogen and argon adsorption, J. Colloid Interface Sci. 207 (1998) 159–169.
[28] P.I. Ravikovitch, G.L. Haller, A.V. Neimark, Density functional theory model for calculating pore size distributions: pore structure of nanoporous catalysts, Adv. Colloid Interface Sci. 76–77 (1998) 203–226.
[29] G. Kupgan, T.P. Liyana-Arachchi, C.M. Colina, NLDFT pore size distribution in amorphous microporous materials, Langmuir 33 (2017), 11138-1114.
[30] P.I. Ravikovitch, A. Vishnyakov, R. Russo, A.V. Neimark, Unified approach to pore size characterization of microporous carbonaceous materials from N_2, Ar, and CO_2 adsorption isotherms, Langmuir 16 (2000) 2311–2320.
[31] J. Jagiello, J.P. Olivier, A simple two-dimensional NLDFT model of gas adsorption in finite carbon pores: application to pore structure analysis, J. Phys. Chem. C 113 (2009) 19382–19385.
[32] A.V. Neimark, Y. Lin, P.I. Ravikovitch, M. Thommes, Quenched solid density functional theory and pore size analysis of micro-mesoporous carbons, Carbon 47 (2009) 1617–1628.
[33] E.C. Oguz, M. Marechal, F. Ramiro-Manzano, I. Rodriguez, R. Messina, F.J. Meseguer, H. Löwen, Packing confined hard spheres denser with adaptive prism phases, Phys. Rev. Lett. 109 (2012), 218301-1–5.
[34] M. Schwaab, E.C. Biscaia, J.L. Monteiro, J.C. Pinto, Nonlinear parameter estimation through particle swarm optimization, Chem. Eng. Sci. 63 (2008) 1542–1552.
[35] J.W. Lee, W.G. Shim, M.S. Yang, H. Moon, Adsorption isotherms of polar and nonpolar organic compounds on MCM-48 at (303.15, 313.15, and 323.15) K, J. Chem. Eng. Data 49 (2004) 502–509.
[36] K. Schumacher, P.I. Ravikovitch, A.D. Chesne, A.V. Neimark, K.K. Unger, Characterization of MCM-48 materials, Langmuir 16 (2000) 4648–4654.
[37] P. Weniger, W. Kalkreuth, A. Busch, B.M. Krooss, High-pressure methane and carbon dioxide sorption on coal and shale samples from the Paraná Basin, Brazil, Int. J. Coal Geol. 84 (2010) 190–205.
[38] R. Heller, M. Zoback, Adsorption of methane and carbon dioxide on gas shale and pure mineral samples, J. Unconventional Oil Gas Resour. 8 (2014) 14–24.
[39] S. Himeno, T. Komatsu, S. Fujita, High-pressure adsorption equilibria of methane and carbon dioxide on several activated carbons, J. Chem. Eng. Data 50 (2005) 369–376.
[40] F. Dreisbach, R. Staudt, J.U. Keller, High pressure adsorption data of methane, nitrogen, carbon dioxide and their binary and ternary mixture on activated carbon, Adsorption 5 (1999) 215–227.
[41] M. Sudibandriyo, Z. Pan, J.E. Fitzgerald, R.L. Robinson Jr., K.A.M. Gasem, Adsorption of methane, nitrogen, carbon dioxide, and their binary mixtures on dry activated carbon at 318.2 K and pressures up to 13.6 MPa, Langmuir 19 (2003) 5323–5331.
[42] S. Brunauer, L.S. Deming, W.E. Deming, E. Teller, On a theory of the van der Waals adsorption of gases, J. Am. Chem. Soc. 62 (1940) 1723–1732.
[43] J. Rouquerol, D. Avnir, C.W. Fairbridge, D.H. Everett, J.H. Haynes, N. Pernicone, J.D.F. Ramsay, K.S.W. Sing, K.K. Unger, Recommendations for the characterization of porous solids, Pure Appl. Chem. 66 (1994) 1739–1758.
[44] G. Chen, S. Lu, J. Zhang, Q. Xue, T. Han, H. Xue, S. Tian, J. Li, C. Xu, M. Pervukhina, Keys to linking GCMC simulations and shale gas adsorption experiments, Fuel 199 (2017) 14–21.
[45] Z. Li, Z. Jin, A. Firoozabadi, Phase behavior and adsorption of pure substances and mixtures and characterization in nanopore structures by density functional theory, SPE J. 19 (2014) 1096–1109.
[46] S.I. Sandler, The generalized van der Waals partition function. I. Basic theory, Fluid Phase Equilib. 19 (1985) 233–257.
[47] L. Travalloni, M. Castier, F.W. Tavares, Phase equilibrium of fluids confined in porous media from an extended Peng-Robinson equation of state, Fluid Phase Equilib. 362 (2014) 335–341.